IEEE Access
Multidisciplinary ⋮ Rapid Review ⋮ Open Access Journal

Received September 10, 2020, accepted September 18, 2020, date of publication September 22, 2020, date of current version October 5, 2020.

Digital Object Identifier 10.1109/ACCESS.2020.3025969

Extended State Observer Based Robust Position Tracking Control Using Nonlinear Damping Gain for Quadrotors With External Disturbance

SESUN YOU[1], KWANYEON KIM[2], JUN MOON[3], (Senior Member, IEEE), AND WONHEE KIM[2], (Member, IEEE)

[1]Department of Energy Systems Engineering, Chung-Ang University, Seoul 06974, South Korea
[2]School of Energy Systems Engineering, Chung-Ang University, Seoul 06974, South Korea
[3]Department of Electrical Engineering, Hanyang University, Seoul 04763, South Korea

Corresponding author: Wonhee Kim (whkim79@cau.ac.kr)

This work was supported in part by the National Research Foundation of Korea (NRF) through the Energy Cloud Research and Development Program funded by the Ministry of Science, ICT (MSIT) under Grant 2019M3F2A1073313, and in part by the Ministry of Trade, Industry and Energy (MOTIE), South Korea, through the Research Program, Improved Development of an Electric Power Steering System (EPS) to Enhance the Driving Stability of Micro Electric Vehicle, under Grant 20007447.

ABSTRACT We propose an extended-state-observer (ESO)-based robust position tracking control method using nonlinear damping gain to improve the control performance under external disturbances and parameter uncertainties for quadrotors. The proposed method consists of an ESO and a nonlinear damping controller (NDC). The ESO is designed to estimate full state and disturbance. The external disturbance, velocity dynamics, and the uncertainty of the input parameter are lumped in the disturbance. The NDC is developed via backstepping procedure to suppress the output tracking error according to the disturbance estimation error. The proposed method is simple and robust against external disturbance and parameter uncertainties. In addition, only the nominal value of the input gain parameters are required. The closed-loop stability is proven by using the input-to-state stability property. The position tracking performance of proposed method was verified by performing hardware-in-the-loop simulations using a quadrotor platform.

INDEX TERMS Extended state observer (ESO), nonlinear damping contol (NDC), quadrotor, robust position control, hardware-in-the-loop-simulation (HILS).

I. INTRODUCTION

Quadrotors are a type of the unmanned aerial vehicle. In recent years, quadrotors have attracted considerable interest owing to their various advantages, such as simplicity in structure, vertical take-off and landing capability, hover capability, rapid maneuverability, and agility. In addition, quadrotors are more effective than conventional helicopters in terms of economics, safety, and size. Applying these advantages, quadrotors have been widely used in fields, such as military services, surveillance, fire fighting, and environmental monitoring [1]–[3]. To accomplish the mission of these industrial applications, the high precision attitude and position control should be necessary. However, it is difficult to control quadrotors for autonomous flight due to high nonlinearity, strong coupled states, and open-loop instability. A quadrotor is a typical underactuated system which the number of actuators is less than the degrees of freedom. And obtaining the exact values of parameters such as moment of inertia, lift and drag coefficients is very hard. In addition, external disturbances, such as fickle winds, degrade the control performance of quadrotors because of their small and light weight [28].

Proportional-integral-derivative controllers and linear quadratic regulators have been widely used in representative linear control methods [4]–[6]. However, the control performance may deteriorate at outside of the region around the equilibrium point owing to strong nonlinear terms. Therefore, various nonlinear control methods have been developed for quadrotors [7]–[25]. Feedback linearization methods were developed to eliminate nonlinear term using feedback [9], [10]. The Lyapunov redesign method was proposed to improve the stability from effect of high order nonlinear term and unmodeled dynamics [11]–[13].

The associate editor coordinating the review of this manuscript and approving it for publication was Dipankar Deb.

Sliding mode control methods were proposed to improve the robustness in finite time [14]–[18]. Adaptive control methods were developed to compensate for parameter uncertainties such as mass variation [20]–[25]. Even though these methods improve stability and control performance, the external disturbance such as wind gust was not compensated for.

Disturbance observer (DOB)-based control algorithms have been developed via backstepping procedure to compensate for the external disturbances that do not satisfy matching conditions [26]–[28]. Adaptive fuzzy based control methods have been developed to compensate for the disturbances and uncertainties [29]–[31]. However, the full state feedback is required to apply these methods. Thus, an extended state observer (ESO) has been developed to estimate full state and disturbance. Various ESO-based control methods have been implemented for quadrotors [32]–[35]. Only external disturbances or partial unmodeled dynamics, such as the gyroscopic effect are considered as the disturbance in attitude dynamics. A nonlinear robust compensation method was developed using robust filter [36]. A finite-time backstepping controller was proposed to guarantee the finite-time convergence using an augmented sliding mode observer [37]. A nonlinear augmented observer-based control was proposed to reject the stochastic noise based on frequency analysis [38]. In [38], the external disturbance and model dynamics were lumped into disturbance. In practice, it is difficult to estimate the disturbance which include the external disturbance and model dynamics. Therefore, a high observer gain is necessary to obtain precise disturbance estimation performance. However, a high observer gain may result in amplifying high frequency measurement noise and inducing input saturation [39], [40].

In this study, we propose an ESO-based robust position tracking control method using nonlinear damping gain to improve the control performance under external disturbances and parameter uncertainties for quadrotors. The proposed method consists of an ESO and a nonlinear damping controller (NDC). The ESO is designed to estimate full state and disturbances. The disturbance is defined as including external disturbance, model dynamics and the uncertainties of input parameters. The NDC is developed via backstepping procedure to suppress output tracking error according to disturbance estimation error. Although poor disturbance estimation performance may degrade the position tracking performance, the nonlinear damping gain increases to enhance the damping effect. The proposed method is simple and robust against external disturbance and parameter uncertainties. In addition, only nominal values of input gain parameters are required. The closed-loop stability is investigated to prove that the proposed method ensures the uniform ultimate boundedness of position and attitude tracking errors using the input-to-state stability (ISS) property. The position tracking performance of proposed method is verified by performing hardware-in-the-loop-simulation (HILS) using a quadrotor platform.

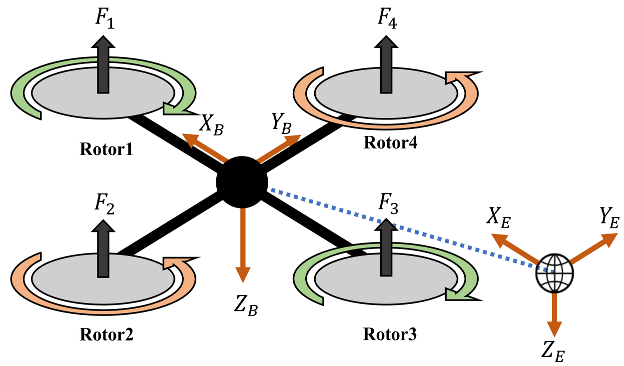

FIGURE 1. Quadrotors model.

The main contributions of this study are as follows:

- An NDC is designed to suppress the tracking error according to the disturbance estimation error.
- Only the nominal value of the input gain parameters are required for the proposed method.
- The proposed method is simple and robust against external disturbance and parameter uncertainties.

II. MATHEMATICAL MODEL AND PROBLEM FORMULATION

In this section, the dynamics of quadrotors is explained [15]. A quadrotor can be simplified by considering only the cross-shaped rigid frame with four rotors. The simplified model of the quadrotor is shown in Fig 1. The inertia frame with respect to earth is defined as $P_E = [X_E, Y_E, Z_E]$, and the body-fixed frame with respect to body is defined as $P_B = [X_B, Y_B, Z_B]$. Define $\xi = [\phi, \theta, \psi]^T$ and $\omega = [p, q, r]^T$, where ϕ, θ, and ψ denote the angle of roll, pitch, and yaw with respect to the inertia frame, respectively, and p, q, and r denote the angular velocity of roll, pitch, and yaw with respect to the body-fixed frame, respectively. The coordinate transform matrix, R_t, from P_B to P_E can be obtained as follows:

$$\underbrace{\begin{bmatrix} C\psi C\theta & C\psi S\theta S\phi - S\psi C\phi & C\psi S\theta C\phi + S\psi S\phi \\ S\psi C\theta & S\psi S\theta S\phi + C\psi C\phi & S\psi S\theta C\phi - C\psi S\phi \\ -S\theta & C\theta S\phi & C\theta C\phi \end{bmatrix}}_{R_t} \tag{1}$$

where $C* = \cos(*)$ and $S* = \sin(*)$. The relationship between $\dot{\xi}$ and ω can be represented using the derivatives of R_t with respect to time as follows:

$$\omega = \underbrace{\begin{bmatrix} 1 & 0 & -S\theta \\ 0 & C\phi & C\theta S\phi \\ 0 & -S\phi & C\theta C\phi \end{bmatrix}}_{W(\xi)} \dot{\xi}. \tag{2}$$

The dynamics of the quadrotor can be obtained by using the Newton-Euler equations as follows:

$$\begin{aligned} M\ddot{P} &= e_3 Mg - F_A + R_t F \\ \omega &= W(\xi)\dot{\xi} \\ J\dot{\omega} &= -\omega \times J\omega - \tau_{gyro} - \tau_A + \tau \end{aligned} \tag{3}$$

where $P = [x, y, z]^T$ is the absolute linear position of the quadrotor, $e_3 = [0, 0, 1]^T$ is the unit vector, M is the mass diagonal matrix of the quadrotor, F_A and τ_A are the aero-drag force matrices of translational motion and rotational motion respectively, τ_{gyro} is the gyroscopic moment, and J is the inertia diagonal matrix of the quadrotor. $F \in R^1$ and $\tau \in R^3$ are control inputs which are defined as follows:

$$\begin{bmatrix} F \\ \tau \end{bmatrix} = \begin{bmatrix} U1 \\ U2 \\ U3 \\ U4 \end{bmatrix} = \begin{bmatrix} k(\Omega_1^2 + \Omega_2^2 + \Omega_3^2 + \Omega_4^2) \\ lk(\Omega_4^2 - \Omega_2^2) \\ lk(\Omega_3^2 - \Omega_1^2) \\ b(\Omega_2^2 + \Omega_4^2 - \Omega_1^2 - \Omega_3^2) \end{bmatrix} \tag{4}$$

where k is the drag force coefficient, b is the lift coefficient, l is the arm length, and Ω_a $a \in [1, 4]$ denotes the rotor speeds of the front, right, rear, and left rotors. The gyroscopic moment, τ_{gyro}, is expressed as

$$\tau_{gyro} = J_r(\omega \times e_3)\bar{\Omega} \tag{5}$$

where J_r is the inertia of the rotor, and the $\bar{\Omega}$ is expressed as $\bar{\Omega} = \Omega_1 + \Omega_3 - \Omega_2 - \Omega_4$. For representing the state-space equation, state X is defined as

$$\begin{aligned} X &= [x_1, \cdots, x_{12}]^T \\ &= [\phi, \dot{\phi}, \theta, \dot{\theta}, \psi, \dot{\psi}, z, \dot{z}, x, \dot{x}, y, \dot{y}]^T \in \mathbb{R}^{12}. \end{aligned} \tag{6}$$

The dynamics of the quadrotor including external disturbances can be represented in a state-space, $\dot{X} = f(X, U)$ where

$$f(X,U) = \begin{bmatrix} x_2 \\ a_1x_4x_6 - a_2x_4\bar{\Omega} - \dfrac{\tau_{Ax}}{I_x} + \dfrac{d_\phi}{I_x} + b_1U2 \\ x_4 \\ a_3x_2x_6 + a_4x_2\bar{\Omega} - \dfrac{\tau_{Ay}}{I_y} + \dfrac{d_\theta}{I_y} + b_2U3 \\ x_6 \\ a_5x_4x_2 - \dfrac{\tau_{Az}}{I_z} + \dfrac{d_\psi}{I_z} + b_3U4 \\ x_8 \\ g + \dfrac{1}{m}[F_{Az} + d_z] + b_4U1 \\ x_{10} \\ \dfrac{1}{m}[-F_{Ax} + d_x] + b_5u_x \\ x_{12} \\ \dfrac{1}{m}[-F_{Ay} + d_y] + b_6u_y \end{bmatrix}$$

$$\begin{aligned} U &= [u_1, \cdots, u_6]^T \\ &= \begin{bmatrix} U2 & U3 & U4 & U1 & u_x & u_y \end{bmatrix}^T \end{aligned} \tag{7}$$

and $a_1 = (I_y - I_z)/I_x$, $a_2 = J_r/I_x$, $a_3 = (I_z - I_x)/I_y$, $a_4 = J_r/I_y$, $a_5 = (I_x - I_y)/I_z$, $b_1 = 1/I_x$, $b_2 = 1/I_y$, $b_3 = 1/I_z$, $b_4 = -(\cos\theta\cos\phi)/m$, $b_5 = -U1/m$ and $b_6 = U1/m$, U is the input matrix, $U1$ is thrust force, $U2$, $U3$, and $U4$ are the rotational torques with respect to roll, pitch, and yaw, respectively, m is the mass of the quadrotor, $I_{x,y,z}$ is the inertial diagonal matrix of the quadrotor, and $d_{ext} = [d_x, d_y, d_z, d_\phi, d_\theta, d_\psi]^T$ denotes external disturbances. u_x and u_y are the orientations of $U1$, and they are defined as follows:

$$\begin{aligned} u_x &= (\sin\psi\sin\phi + \cos\psi\sin\theta\cos\phi) \\ u_y &= (\cos\psi\sin\phi - \sin\psi\sin\theta\cos\phi). \end{aligned} \tag{8}$$

u_x and u_y are used as the virtual control inputs for the translational system to compute x_{1_d} and x_{3_d}. The uncertainty Δb_i and the nominal value b_i^o of b_i $i \in [1, 6]$ are defined as

$$b_i = \Delta b_i + b_i^o. \tag{9}$$

The disturbances, d_i $i \in [1, 6]$, which include the external disturbances, dynamics, and the uncertainties of input parameters, are defined as

$$\begin{aligned} d_1 &= a_1x_4x_6 - a_2x_4\bar{\Omega} - \frac{\tau_{Ax}}{I_x} + \frac{d_\phi}{I_x} + \Delta b_1U2 \\ d_2 &= a_3x_2x_6 + a_4x_2\bar{\Omega} - \frac{\tau_{Ay}}{I_y} + \frac{d_\theta}{I_y} + \Delta b_2U3 \\ d_3 &= a_5x_4x_2 - \frac{\tau_{Az}}{I_z} + \frac{d_\psi}{I_z} + \Delta b_3U4 \\ d_4 &= g + \frac{1}{m}[F_{Az} + d_z] + \Delta b_4U1 \\ d_5 &= \frac{1}{m}[-F_{Ax} + d_x] + \Delta b_5u_x \\ d_6 &= \frac{1}{m}[-F_{Ay} + d_y] + \Delta b_6u_y. \end{aligned} \tag{10}$$

For simplification, (7) can be rewritten as

$$f(X,U) = \begin{bmatrix} x_2 \\ d_1 + b_1^oU2 \\ x_4 \\ d_2 + b_2^oU3 \\ x_6 \\ d_3 + b_3^oU4 \\ x_8 \\ d_4 + b_4^oU1 \\ x_{10} \\ d_5 + b_5^ou_x \\ x_{12} \\ d_6 + b_6^ou_y \end{bmatrix}. \tag{11}$$

III. EXTENDED STATE OBSERVER DESIGN

The ESO is designed to estimate full state and disturbances. The extended state variable vector, $X_e = [x_{e_1}, \cdots, x_{e_{18}}]^T \in \mathbb{R}^{18}$, and the estimation state variable vector, $\hat{X}_e = [\hat{x}_{e_1}, \cdots, \hat{x}_{e_{18}}]^T \in \mathbb{R}^{18}$, are defined as follows:

$$\begin{aligned} X_e &= [\phi, \dot{\phi}, d_1, \theta, \dot{\theta}, d_2, \psi, \dot{\psi}, d_3, z, \dot{z}, d_4, x, \dot{x}, d_5, y, \dot{y}, d_6]^T \\ \hat{X}_e &= [\hat{\phi}, \hat{\dot{\phi}}, \hat{d}_1, \hat{\theta}, \hat{\dot{\theta}}, \hat{d}_2, \hat{\psi}, \hat{\dot{\psi}}, \hat{d}_3, \hat{z}, \hat{\dot{z}}, \hat{d}_4, \hat{x}, \hat{\dot{x}}, \hat{d}_5, \hat{y}, \hat{\dot{y}}, \hat{d}_6]^T. \end{aligned} \tag{12}$$

The ESO is designed as

$$\dot{\hat{X}}_e = A_o\hat{X}_e + B_oU + LC(X_e - \hat{X}_e) \tag{13}$$

where

$$A_o = \begin{bmatrix} I_o & 0_{3\times3} & 0_{3\times3} & \cdots & 0_{3\times3} \\ 0_{3\times3} & I_o & 0_{3\times3} & \cdots & 0_{3\times3} \\ \vdots & & \ddots & & \vdots \\ 0_{3\times3} & & & \cdots & I_o \end{bmatrix} \in \mathbb{R}^{18\times18}$$

$$I_o = \begin{bmatrix} 0 & 1 & 0 \\ 0 & 0 & 1 \\ 0 & 0 & 0 \end{bmatrix} \in \mathbb{R}^{3\times3}$$

$$B_o = \begin{bmatrix} B_1 & 0_{3\times1} & 0_{3\times1} & \cdots & 0_{3\times1} \\ 0_{3\times1} & B_2 & 0_{3\times1} & \cdots & 0_{3\times1} \\ \vdots & & \ddots & & \vdots \\ 0_{3\times1} & & \cdots & & B_6 \end{bmatrix} \in \mathbb{R}^{18\times6}$$

$$B_i = \begin{bmatrix} 0 & b_i^o & 0 \end{bmatrix}^T \in \mathbb{R}^{3\times1}, \quad i \in [1, 6]$$

$$L = \begin{bmatrix} L_1 & 0_{3\times1} & 0_{3\times1} & \cdots & 0_{3\times1} \\ 0_{3\times1} & L_4 & 0_{3\times1} & \cdots & 0_{3\times1} \\ \vdots & & \ddots & & \vdots \\ 0_{3\times1} & & \cdots & & L_{16} \end{bmatrix} \in \mathbb{R}^{18\times6}$$

$$L_s = \begin{bmatrix} l_s & l_{s+1} & l_{s+2} \end{bmatrix}^T \in \mathbb{R}^{3\times1}, \quad s \in \{1, 4, 7, 10, 13, 16\}$$

$$C = \begin{bmatrix} C_o & 0_{1\times3} & \cdots & 0_{1\times3} \\ 0_{1\times3} & C_o & \cdots & 0_{1\times3} \\ \vdots & & \ddots & \vdots \\ 0_{1\times3} & 0_{1\times3} & \cdots & C_o \end{bmatrix} \in \mathbb{R}^{6\times18}$$

$$C_o = \begin{bmatrix} 1 & 0 & 0 \end{bmatrix} \in \mathbb{R}^{1\times3}$$

and L is the observer gain matrix. The estimation error matrix of the extended state is defined as

$$\tilde{X}_e = X_e - \hat{X}_e. \tag{14}$$

The dynamics of $\tilde{X}_e$ becomes

$$\dot{\tilde{X}}_e = \underbrace{(A_o - LC)}_{A_{eo}}\tilde{X}_e + B_d\delta \tag{15}$$

where

$$\delta = \begin{bmatrix} \delta_1 & \delta_2 & \delta_3 & \delta_4 & \delta_5 & \delta_6 \end{bmatrix}^T \in \mathbb{R}^6$$

$$B_d = \begin{bmatrix} I_d & 0_{3\times1} & \cdots & 0_{3\times1} \\ 0_{3\times1} & I_d & \cdots & 0_{3\times1} \\ \vdots & & \ddots & \vdots \\ 0_{3\times1} & 0_{3\times1} & \cdots & I_d \end{bmatrix} \in \mathbb{R}^{18\times6}$$

$$I_d = \begin{bmatrix} 0 & 0 & 1 \end{bmatrix}^T \in \mathbb{R}^{3\times1} \tag{16}$$

and δ_i, $i \in [1, 6]$ is the derivative of the disturbances. In most practical systems such as quadrotors, vehicles, hydraulic actuators, and motors, all state variables and external disturbances are physically bounded, as the inputs are bounded in practical system [42]. Thus, assumptions 1 and 2 are reasonable.

Assumption 1: The disturbance, $d \in \mathbb{R}^6$, and the derivative of the disturbance, $\delta \in \mathbb{R}^6$, are bounded. Thus, the upper bound of $|\delta|$, represented by $\delta_{\max} \in \mathbb{R}^6$, is positive such that $\sup_{0\le t\le\infty} |\delta(t)| = \delta_{\max}$.

Assumption 2: $\tilde{X}_e \in B_x = \|\tilde{X}_e\|_2 \le b_x$, where b_x is an unknown positive constant.

Theorem 1: Under Assumptions 1 and 2, if the observer gain matrix, L, is selected such that $A_{eo} = A_o - LC$ matrix is a Hurwitz matrix, the perturbation term satisfies the condition as

$$|\delta_i| \le \delta_{\max} < \sqrt{\frac{\lambda_{\min}(P_o)}{\lambda_{\max}(P_o)}}\frac{\eta b_x}{2\lambda_{\max}(P_o)} \tag{17}$$

for all $t > 0$, $\tilde{X}_e \in B_x$ and positive constant $\eta < 1$, where $P_o > 0$ is positive definite such that $A_{eo}^T P_o + P_o A_{eo} = -I$, $\lambda_{\max}(P_o)$ and $\lambda_{\min}(P_o)$ are the maximum and minimum eigenvalues of P_o, respectively. Then, for all $\|\tilde{X}_e(t_o)\| < \sqrt{(\lambda_{\min}(P_o))/(\lambda_{\max}(P_o))}b_x$. $\tilde{X}_e(t)$ satisfies

$$\begin{aligned} &\|\tilde{X}_e(t)\|_2 \le k\exp[\rho(t-t_o)]\|\tilde{X}_e(t_o)\| \quad \forall t_o \le t < t_o + T \\ &\|\tilde{X}_e(t)\|_2 \le k\frac{2\lambda_{\max}(P_o)\delta_{\max}}{\eta} \quad \forall t \ge t_o + T \end{aligned} \tag{18}$$

for some finite T, where $k = \sqrt{(\lambda_{\max}(P_o))/(\lambda_{\min}(P_o))}$ and $\rho = -(1-\eta)$.

Proof: We define the Lyapunov candidate function V_o as

$$V_o = \tilde{X}_e^T P_o \tilde{X}_e. \tag{19}$$

The derivative of V_o with respect to time is

$$\begin{aligned} \dot{V}_o &= \tilde{X}_e^T[A_{eo}^T P_o + P_o A_{eo}]\tilde{X}_e + 2\tilde{X}_e^T P_o B_d \delta \\ &\le -\|\tilde{X}_e(t)\|_2^2 + 2\delta_{\max}\|P_o\|_2\|\tilde{X}_e(t)\|_2 \\ &= -(1-\eta)\|\tilde{X}_e(t)\|_2^2 - \eta\|\tilde{X}_e(t)\|_2^2 \\ &\quad + 2\delta_{\max}\lambda_{\max}(P_o)\|\tilde{X}_e(t)\|_2 \\ &\le -(1-\eta)\|\tilde{X}_e(t)\|_2^2 \quad \text{for } \forall \|\tilde{X}_e(t)\|_2 \ge \frac{2\lambda_{\max}(P_o)\delta_{\max}}{\eta}. \end{aligned} \tag{20}$$

The proof is completed by applying Theorem 4.18 in [43]. ♢

IV. NONLINEAR DAMPING CONTROLLER DESIGN

This section describes the design of the NDC via backstepping to suppress the position tracking error when estimation error increases owing to the disturbances. As the dynamics of the quadrotor consists of six second-order single-input-single-output systems (11), the general form is represented as second-order system. The tracking error, denoted by $e = [e_1\ e_2\ \cdots\ e_{11}\ e_{12}]^T \in \mathbb{R}^{12}$, is defined as

$$e_i = x_i - x_{i_d}, \quad i \in [1, 12] \tag{21}$$

where x_{i_d} is yet to be defined. The estimated tracking error $\hat{e}_i$ is defined as

$$\hat{e}_i = \hat{x}_i - x_{i_d}, \quad i \in [1, 12]. \tag{22}$$

The tracking error dynamics can be defined as

$$\begin{aligned} \dot{e}_i &= e_{i+1} + x_{i+1_d} - \dot{x}_{i_d}, \quad i \in \{1, 3, 5, 7, 9, 11\} \\ \dot{e}_{i+1} &= b_i^o u_j + d_i - \dot{x}_{i+1_d}, \quad j = [1, 6]. \end{aligned} \tag{23}$$

To ensure the boundedness of the tracking error e_i, the desired state and NDC input are designed as

$$x_{i+1_d} = -k_i e_i + \dot{x}_{i_d}, \quad i \in \{1,3,5,7,9,11\},\ j = [1,6]$$
$$u_j = \underbrace{\frac{1}{b_i^o}\left(-k_{i+1}e_{i+1} + \dot{x}_{i+1_d} - \hat{d}_i\right)}_{u_a}$$
$$\underbrace{\frac{1}{b_i^o}\left(-\left(k_{d_i}\sqrt{\hat{e}_i^2+\gamma_i}+k_{d_{i+1}}\sqrt{\hat{d}_i^2+\gamma_{i+1}}\right)e_{i+1}\right)}_{u_b} \quad (24)$$

where control gains $k_i, k_{i+1}, k_{d_i}, k_{d_{i+1}}, \gamma_i$, and γ_{i+1} are positive constants. The control input u_j in (24) consists of two parts, i.e., the stabilization part, u_a, and the nonlinear damping part, u_b. The nonlinear damping part is considered to suppress the tracking error e_i according to disturbance estimation error. The disturbances include the external disturbances, unmodeled dynamics, and parameter uncertainties. Thus, it is difficult to accurately estimate d_i when the disturbance increases. Generally, if u_a is used exclusively, the tracking error, e_i, increases as much as the estimation error of disturbance, $\tilde{d}_i$. The nonlinear damping gain, u_b, can improve the damping effect of $\tilde{d}_i$ to e_i, when $\hat{e}_i$ and $\hat{d}_i$ increase, because $\tilde{d}_i$ becomes larger with the increase of d_i. We define nonlinear damping gain $k_d(\hat{e}_i, \hat{d}_i)$ as

$$k_d(\hat{e}_i, \hat{d}_i) = \left(k_{d_i}\sqrt{\hat{e}_i^2+\gamma_i} + k_{d_{i+1}}\sqrt{\hat{d}_i^2+\gamma_{i+1}}\right). \quad (25)$$

Theorem 2: Consider the tracking error dynamics (23). If the proposed control input (24) is applied to (23), the tracking error dynamics (23) is the serial interconnected system of ISS systems with the following property:

$$|e_i(t)| \le \exp\left(-\frac{k_i}{2}t\right)|e_i(0)| + \frac{2}{k_i}\sup_{0\le\tau\le t}|e_{i+1}(\tau)|$$
$$|e_{i+1}(t)| \le \exp\left(-\frac{k_{i+1}}{2}t\right)|e_{i+1}(0)| + \sup_{0\le\tau\le t}\sigma(\tau) \quad (26)$$

where

$$\sigma = \frac{|\tilde{d}_i|}{0.5k_{i+1} + k_d(\hat{e}_i, \hat{d}_i)}. \quad (27)$$

Proof: The tracking error dynamics (23) with the control law (24) becomes

$$\dot{e}_i = -k_i e_i + e_{i+1}, \quad i \in \{1,3,5,7,9,11\}$$
$$\dot{e}_{i+1} = -k_{i+1}e_{i+1} - k_d(\hat{e}_i, \hat{d}_i)e_{i+1} + \tilde{d}_i. \quad (28)$$

From (28), the derivative of $\frac{e_{i+1}^2}{2}$ becomes

$$\frac{d}{dt}\left(\frac{e_{i+1}^2}{2}\right)$$
$$= -k_{i+1}e_{i+1}^2 - k_d(\hat{e}_i, \hat{d}_i)e_{i+1}^2 + \tilde{d}_i e_{i+1}$$
$$\le -\frac{k_{i+1}}{2}e_{i+1}^2 - \left(\frac{k_{i+1}}{2} + k_d(\hat{e}_i, \hat{d}_i)\right)|e_{i+1}|(|e_{i+1}| - \sigma)$$
$$\le -\frac{k_{i+1}}{2}e_{i+1}^2 \quad \forall |e_{i+1}| \ge \sigma. \quad (29)$$

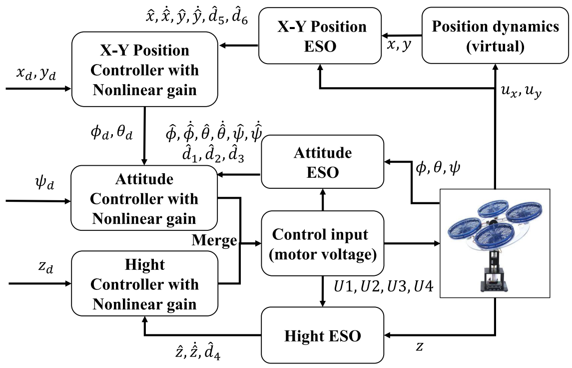

FIGURE 2. Schematic of the HILS test.

We can derive the following result using [[44], Th. C.2]:

$$|e_{i+1}(t)| \le \exp\left(-\frac{k_{i+1}}{2}t\right)|e_{i+1}(0)| + \sup_{0\le\tau\le t}\sigma(\tau). \quad (30)$$

From (30), we can show that the relationship between e_{i+1} and σ satisfies the ISS property. Similarly, the derivative of $\frac{e_i^2}{2}$ becomes

$$\frac{d}{dt}\left(\frac{e_i^2}{2}\right) = -k_i e_i^2 + e_i e_{i+1}$$
$$\le -\frac{k_i}{2}e_i^2 - \left(\frac{k_i}{2}\right)|e_i|(|e_i| - \frac{2}{k_i}|e_{i+1}|)$$
$$\le -\frac{k_i}{2}e_i^2 \quad \forall |e_i| \ge \frac{2}{k_i}|e_{i+1}|. \quad (31)$$

Then,

$$|e_i(t)| \le \exp\left(-\frac{k_i}{2}t\right)|e_i(0)| + \frac{2}{k_i}\sup_{0\le\tau\le t} e_{i+1}(\tau). \quad (32)$$

Equation (32) shows that the relationship between e_{i+1} and e_i satisfies the ISS property. From (30) and (32), the ISS property of the overall tracking error system is represented by (26). Thus, the tracking error dynamics (28) is the serial interconnected system of ISS systems. ◊

Remark 1: The expression for σ (27) includes $k_d(\hat{e}_i, \hat{d}_i)$ in the denominator. Therefore, the σ decreases when $\hat{e}_i$ and $\hat{d}_i$ increase because of external disturbance. In other words, the nonlinear damping gain, u_b, suppresses the effects of $|\tilde{d}_i|$ to e_{i+1}. According to the ISS property (26), as $t \to \infty$

$$|e_i(\infty)| \le \frac{2}{k_i}\sup_{0\le\tau\le\infty}|e_{i+1}(\tau)| \le \frac{2}{k_i}\sup_{0\le\tau\le\infty}\sigma(\tau). \quad (33)$$

The tracking error, e_i, can be effectively suppressed even though $|\tilde{d}_i|$ increase.

Remark 2: The schematic of proposed method is shown in Fig 2. As mentioned previously, a quadrotor is a typical underactuated system in which the number of actuators is less than the degrees of freedom. Thus, u_x and u_y are used to generate the desired attitude as the virtual control input for the position control. Based on (8) and simple calculation, x_{1_d} and x_{3_d} can be obtained as

$$\begin{aligned} x_{1_d} &= \arcsin(u_x \sin x_{5_d} + u_y \cos x_{5_d}) \\ x_{3_d} &= \arcsin\left(\frac{u_x \cos x_{5_d} - u_y \sin x_{5_d}}{\cos x_{1_d}}\right). \end{aligned} \quad (34)$$

V. ANALYSIS OF CLOSED-LOOP STABILITY

This section describes closed-loop stability analysis. Note that only the output feedback is available. In (24), the actual states must be substituted with in estimated state. The estimated control input, $\hat{u}_j,\ j = [1, 6]$, is defined as

$$\begin{aligned} \hat{u}_j = &\frac{1}{b_i^o}\left(-k_{i+1}\hat{e}_{i+1} + \dot{x}_{i+1_d} - \hat{d}_i\right) \\ &+ \frac{1}{b_i^o}\left(-\left(k_{d_i}\sqrt{\hat{e}_i^2 + \gamma_i} + k_{d_{i+1}}\sqrt{\hat{d}_i^2 + \gamma_{i+1}}\right)\hat{e}_{i+1}\right). \end{aligned} \quad (35)$$

As the output states are available, the same desired states (24) designed by the backstepping control law are used in (35). The estimated control input (35) is applied to (23), and the closed-loop tracking error dynamics can be obtained as

$$\dot{E}_i = A_{ei}E_i + B_{ei}\xi \quad i \in \{1, 3, 5, 7, 9, 11\} \quad (36)$$

where

$$\begin{aligned} E_i &= \begin{bmatrix} e_i & e_{i+1} \end{bmatrix}^T \\ A_{ei} &= \begin{bmatrix} -k_i & 1 \\ 0 & -k_{i+1} \end{bmatrix} \quad B_{ei} = \begin{bmatrix} 0 \\ 1 \end{bmatrix} \\ \xi &= -k_d(\hat{e}_i, \hat{d}_i)e_{i+1} + d_i - \hat{d}_i + b_i^o\hat{u} - b_i^o u. \end{aligned} \quad (37)$$

The closed-loop system is represented as

$$\dot{E}_i = A_{ei}E_i + B_{ei}\xi \quad (38)$$

$$\dot{\tilde{X}}_e = A_{eo}\tilde{X}_e + B_d\delta \quad i \in \{1, 3, 5, 7, 9, 11\}. \quad (39)$$

As the actual output states and the same desired states are used in u (24) and $\hat{u}$ (35), the positive value, γ, can be defined as

$$\left|d_i - \hat{d}_i + b_i^o\hat{u} - b_i^o u\right| \leq \gamma\|\tilde{X}_e\|. \quad (40)$$

Theorem 3: Consider the closed-loop tracking error dynamics (36). Based on the estimated control input, $\hat{u}$ (35), the closed-loop tracking error dynamics (36) is the serial interconnected system of ISS systems with the following property:

$$\begin{aligned} |e_i(t)| &\leq \exp\left(-\frac{k_i}{2}t\right)|e_i(0)| + \frac{2}{k_i}\sup_{0\leq\tau\leq t}|e_{i+1}(\tau)| \\ |e_{i+1}(t)| &\leq \exp\left(-\frac{k_{i+1}}{2}t\right)|e_{i+1}(0)| + \sup_{0\leq\tau\leq t}\sigma_c(\tau) \end{aligned} \quad (41)$$

where

$$\sigma_c \leq \frac{\gamma\|\tilde{X}_e\|}{0.5k_{i+1} + k_d(\hat{e}_i, \hat{d}_i)}. \quad (42)$$

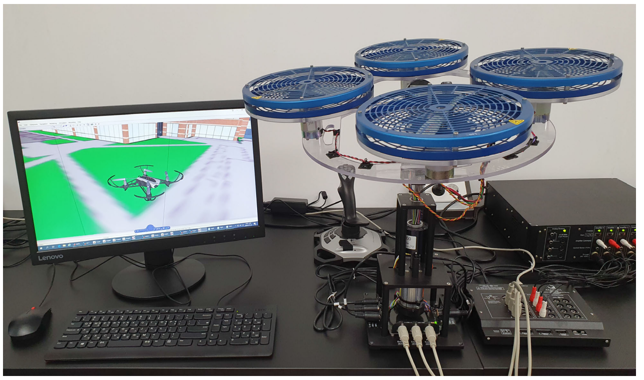

FIGURE 3. Quadrotor HILS testbed.

Proof: In (36), the dynamics of the e_{i+1} with estimated control input becomes

$$\dot{e}_{i+1} = -k_{i+1}e_{i+1} - k_d(\hat{e}_i, \hat{d}_i)e_{i+1} + d_i - \hat{d}_i + b_i^o\hat{u} - b_i^o u. \quad (43)$$

The derivative of $\frac{e_{i+1}^2}{2}$ is obtained from (43), in a similar manner as the aforementioned proof of theorem 2, as follows:

$$\begin{aligned} \frac{d}{dt}\left(\frac{e_{i+1}^2}{2}\right) \leq &-\frac{k_{i+1}}{2}e_{i+1}^2 \\ &-\left(\frac{k_{i+1}}{2} + k_d(\hat{e}_i, \hat{d}_i)\right)|e_{i+1}|(|e_{i+1}| - \sigma_c) \end{aligned} \quad (44)$$

where

$$\begin{aligned} \sigma_c &= \frac{\left|d_i - \hat{d}_i + b_i^o\hat{u} - b_i^o u\right|}{0.5k_{i+1} + k_d(\hat{e}_i, \hat{d}_i)} \\ &\leq \frac{\gamma\|\tilde{X}_e\|}{0.5k_{i+1} + k_d(\hat{e}_i, \hat{d}_i)}. \end{aligned} \quad (45)$$

Thus, equation (30) becomes

$$|e_{i+1}(t)| \leq \exp\left(-\frac{k_{i+1}}{2}t\right)|e_{i+1}(0)| + \sup_{0\leq\tau\leq t}\sigma_c(\tau). \quad (46)$$

From equation (46), we can show that the relationship between e_{i+1} and σ_c satisfies the ISS property. From equation (46) and (32), the ISS property of the overall closed-loop tracking error system is shown in equation (41). Thus, the closed-loop tracking error dynamics (36) is the serial interconnected system of ISS systems. ◊

Remark 3: σ_c (42) depends on the magnitude of estimation error. From equation (17) and (20), the upper bound of estimation error is determined by b_x and eigenvalue of P_o. Generally, as b_x is unknown and constant, a high observer gain is required to decrease the upper bound of estimation error. However, a small b_x and a high observer gain are not necessary to obtain a small σ_c in the proposed method. This is because, when $\hat{e}_i$ and $\hat{d}_i$ increase with $\|\tilde{X}_e\|$, and hence, $k_d(\hat{e}_i, \hat{d}_i)$ increases. In other words, even though estimation performance is insufficient, a small σ_c can be obtained from

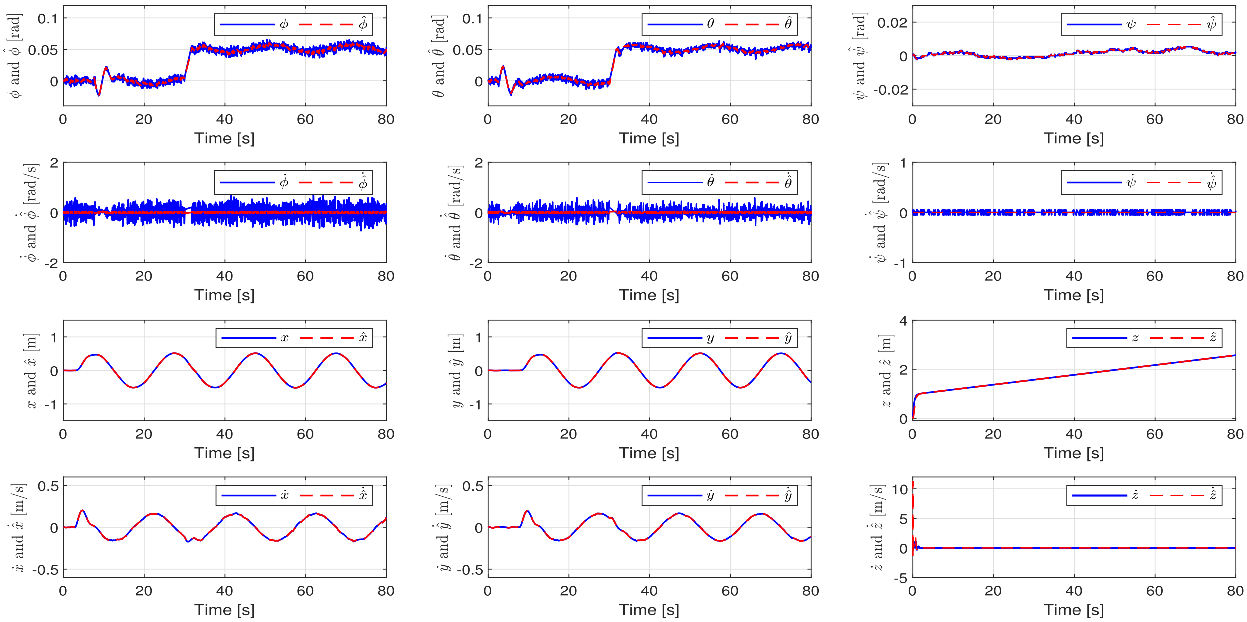

FIGURE 4. State estimation performance of ESO in Case 3.

$k_d(\hat{e}_i, \hat{d}_i)$. Based on the ISS property (41), the closed-loop tracking error system (36) is the serial interconnected system of ISS systems. As $t \to \infty$,

$$|e_i(\infty)| \le \frac{2}{k_i} \sup_{0\le\tau\le\infty} |e_{i+1}(\tau)| \le \frac{2}{k_i} \sup_{0\le\tau\le\infty} \sigma_c(\tau). \quad (47)$$

VI. EXPERIMENTAL RESULTS

The effectiveness of the proposed method is evaluated by performing HILS using quadrotor platform manufactured by Quanser Co., based on MATLAB/Simulink. -The quadrotor is operated by four DC motors. The attitudes are measured by three encoders located on the central axis of the platform. The virtual position dynamics is developed by utilizing Aerospace Simulink toolbox with various realistic environments such as sensor dynamics, gravity, and aerodynamic force. The WGS84 Taylor series gravity model and COESA atmosphere model provided by the Aerospace Simulink toolbox are used to describe the variation in environmental variables with position. The HILS environment testbed is shown in Fig. 3. The nominal parameters of quadrotors are $m = 1.39$ kg, $g = 9.81$ m/s^2, $l = 0.197$ m, $k = 0.0036$ N $\cdot$ m/v, $b = 0.119$ N/v, $I_x = I_y = 5.52 \times 10^{-3}$ kg $\cdot$ m^2, and $I_z = 1.1 \times 10^{-2}$ kg $\cdot$ m^2. The following three cases were examined:

Case 1: Conventional backstepping control.

The control gains were selected as $k_1 = 400$, $k_2 = 1.2$, $k_3 = 400$, $k_4 = 1.2$, $k_5 = 100$, $k_6 = 1$, $k_7 = 2.5$, $k_8 = 1.5$, $k_9 = 2.5$, $k_{10} = 2.5$, $k_{11} = 2.5$, and $k_{12} = 2.5$. The desired states were same as those in (35). The control input is designed as follows:

$$U2 = \frac{1}{b_1^o}\left(-k_2e_2 + \dot{x}_{2_d} - a_1x_4x_6 + a_2x_4\bar{\Omega}\right)$$
$$U3 = \frac{1}{b_2^o}\left(-k_4e_4 + \dot{x}_{4_d} - a_3x_2x_6 - a_4x_2\bar{\Omega}\right)$$
$$U4 = \frac{1}{b_3^o}\left(-k_6e_6 + \dot{x}_{6_d} - a_5x_4x_2\right)$$
$$U1 = \frac{1}{b_4^o}\left(-k_8e_8 + \dot{x}_{8_d} - g\right)$$
$$u_x = \frac{1}{b_5^o}\left(-k_{10}e_{10} + \dot{x}_{10_d}\right)$$
$$u_y = \frac{1}{b_6^o}\left(-k_{12}e_{12} + \dot{x}_{12_d}\right). \quad (48)$$

Case 2: ESO-based backstepping control.

The disturbances, ESO, and control input were defined as in (10), (13), and (35), respectively. The same control gains as those for Case 1 were used. The nonlinear damping gains were selected as $k_{d_i} = 0$, and $\gamma_i = 0$, $i \in [1, 12]$. The ESO gains were selected as $l_s = 53$, $l_{s+1} = 895$ and $l_{s+2} = 4875$, $s \in \{1, 4, 7, 10, 13, 16\}$. The initial values used in the simulations are as follows: $x_i(0) = 0$, $i \in [1, 12]$ and $\hat{x}_{e_j}(0) = 0$, $j \in [1, 18]$.

Case 3: Proposed method.

The disturbances, ESO, and control input are defined as in (10), (13), and (35), respectively. The control gains were selected as $k_1 = 400$, $k_2 = 1$, $k_3 = 400$, $k_4 = 1$, $k_5 = 100$, $k_6 = 1$, $k_7 = 2.5$, $k_8 = 1$, $k_9 = 2.5$, $k_{10} = 2$, $k_{11} = 2.5$, and $k_{12} = 2$. The nonlinear damping gains were selected as $k_{d_i} = 1$, and $\gamma_i = 0.1$, $i \in [1, 12]$. The same ESO gains and initial values are the same as those used in Case 2.

To evaluate the control performance of the proposed method, the control gains of in Case 1 and 2 were set to be larger than the control gains in Case 3. Wind was injected along the X-Y axis as the external disturbance, as follows:

$$d_x = \begin{cases} 0, & 0 \le t \le 30 \\ -0.5(1 - e^{-0.5t}), & 30 \le t. \end{cases}$$

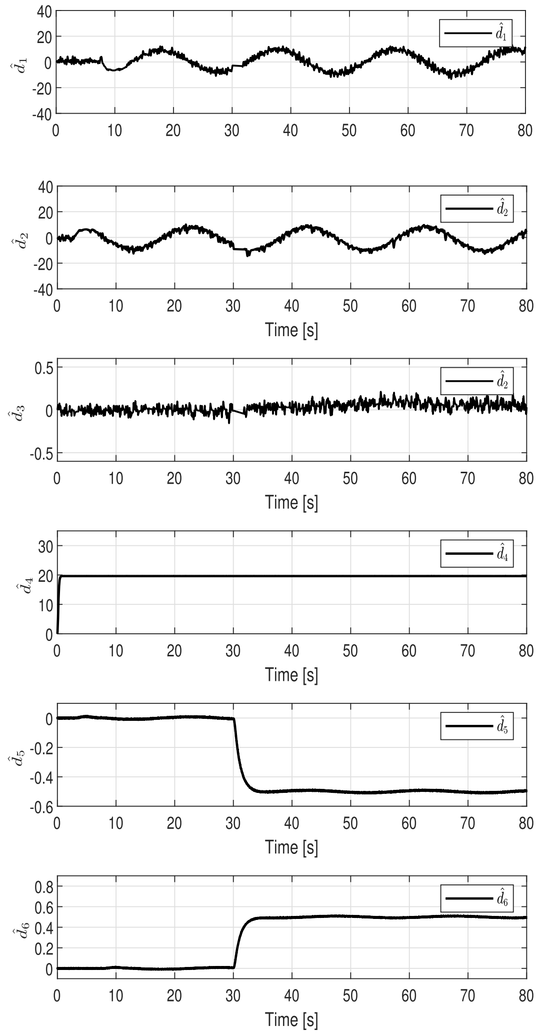

FIGURE 5. Disturbance estimation performance of ESO in Case 3.

$$d_y = \begin{cases} 0, & 0 \le t \le 30 \\ 0.5(1 - e^{-0.5t}), & 30 \le t. \end{cases} \tag{49}$$

The desired positions were defined such as

$$x_d = \begin{cases} 0, & 0 \le t \le 2.5 \\ (1 - e^{-0.5t}) \sin(0.1\pi t), & 2.5 \le t \end{cases}$$
$$y_d = \begin{cases} 0, & 0 \le t \le 7.5 \\ (1 - e^{-0.5t}) \cos(0.1\pi t), & 7.5 \le t \end{cases}$$
$$z_d = \begin{cases} (1 - e^{-0.5t}), & 0 \le t \le 1.5 \\ (1 - e^{-0.5t}) + 0.02t, & 1.5 \le t. \end{cases} \tag{50}$$

The estimation performances of proposed methods are shown in Figs. 4 and 5. The position, velocity, attitude, and angular velocity were accurately estimated using only nominal input gain parameters. The estimated disturbances are shown in Fig. 5. After $t = 30$ s, the offset is observed in d_5 and d_6 because of the injected wind. In addition, a small wave is observed in d_5 and d_6 because of air drag force. The desired and actual trajectories of the quadrotor in Cases 1-3 are shown in Fig. 6. The quadrotor takes off from the origin of the inertial reference frame, P_E, and follows the desired a cylindrical spiral trajectory. The position tracking performance in Case 3 is better than those in Cases 1 and 2. The position tracking errors in Cases 1-3 are shown in Fig. 7. In Case 1, a large steady-state error was observed at $t = 30$ s, because the wind disturbance is not compensated for. In contrast, steady-state

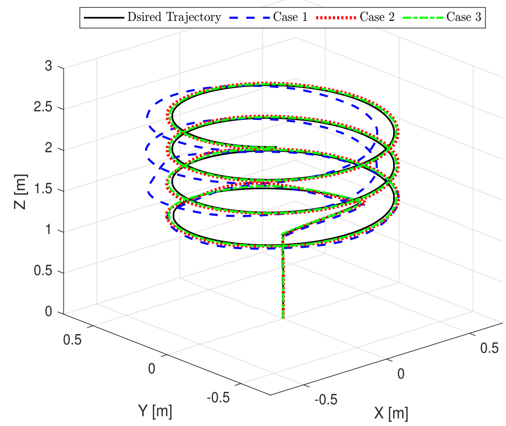

FIGURE 6. Quadrotor trajectories in Cases 1-3.

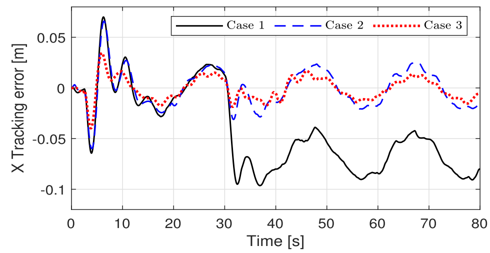

(a) X tracking error

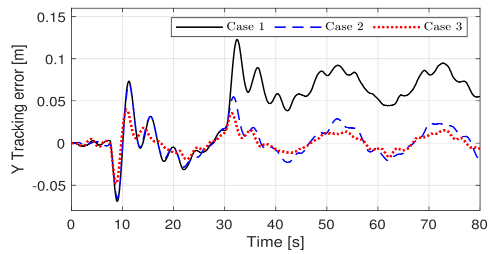

(b) Y tracking error

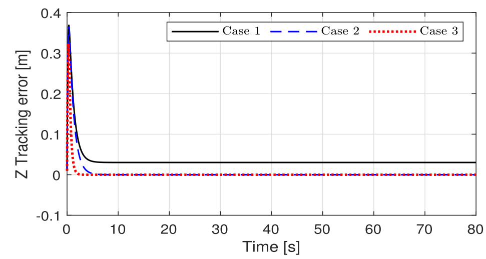

(c) Z tracking error

FIGURE 7. Position tracking errors in Cases 1-3.

errors were significantly reduced by the ESO in Cases 2 and 3. The X tracking error in Case 3 was smaller than that in Case 2 at $t = 46$s, 58s, and 68s, because the nonlinear damping gain (25) was simultaneously increased as much as increment of estimated disturbance. Similar to the X tracking error, the Y tracking error in Case 3 was smaller than that in Case 2, because the increase in external disturbance leads to the increase in nonlinear damping gain (25) in order to indirectly suppress the effect of the disturbance. Z tracking error in Case 3 was reduced by the nonlinear damping gain at hovering. In addition, the settling time for Case 3 was smaller than that for Cases 1 and 2. Videos of the HILS experiments are available at the following web-site.

Case 1: https://youtu.be/FOW_w5BJmLU

Case 2: https://youtu.be/BMs28YT90RY

Case 3: https://youtu.be/_RLg3J2gbRw

Error comparison of Cases 1-3: https://youtu.be/4ZcLG5s DIPk

VII. CONCLUSION

We proposed an ESO-based robust position tracking control method using nonlinear damping gain to improve control performance under external disturbance and parameter uncertainties. The ESO was designed to estimate full state and disturbances, which included the external disturbance, model dynamics and the uncertainties of the input parameters. An NDC was developed via backstepping to suppress position and attitude tracking error according to disturbance estimation error. In experimental results, showed that the ESO accurately estimated the actual states and disturbances. Therefore, the tracking errors of ESO based control methods did not have steady-state error by compensating for estimated disturbance. In addition, when the external disturbance increased, the nonlinear damping gain simultaneously increased to suppress the effect of the disturbance. Therefore, the position tracking error of proposed method was lesser than that of the conventional backstepping control and ESO-based backstepping control with larger control gains. In future work, we will focus on setting up a real quadrotor experimental environment with a position sensor which has centimeter resolution, i.e., real-time kinematic global navigation satellite system, and evaluating the proposed control strategy via outdoor flight experiments.

ACKNOWLEDGMENT

(Sesun You and Kwanyeon Kim are co-first authors.)

REFERENCES

[1] R. Mahony, V. Kumar, and P. Corke, "Multirotor aerial vehicles: Modeling, estimation, and control of quadrotor," *IEEE Robot. Autom. Mag.*, vol. 19, no. 3, pp. 20–32, Sep. 2012.

[2] A. Tayebi and S. McGilvray, "Attitude stabilization of a VTOL quadrotor aircraft," *IEEE Trans. Control Syst. Technol.*, vol. 14, no. 3, pp. 562–571, May 2006.

[3] S. Grzonka, G. Grisetti, and W. Burgard, "A fully autonomous indoor quadrotor," *IEEE Trans. Robot.*, vol. 28, no. 1, pp. 90–100, Feb. 2012.

[4] S. Bouabdallah, A. Noth, and R. Siegwart, "PID vs LQ control techniques applied to an indoor micro quadrotor," in *Proc. IEEE/RSJ Int. Conf. Intell. Robots Syst. (IROS)*, Sep. 2004, pp. 2451–2456.

[5] J. Li and Y. Li, "Dynamic analysis and PID control for a quadrotor," in *Proc. IEEE Int. Conf. Mechatronics Autom.*, Aug. 2011, pp. 573–578.

[6] F. Rinaldi, S. Chiesa, and F. Quagliotti, "Linear quadratic control for quadrotors UAVs dynamics and formation flight," *J. Intell. Robotic Syst.*, vol. 70, nos. 1–4, pp. 203–220, Apr. 2013.

[7] B. Zhao, B. Xian, Y. Zhang, and X. Zhang, "Nonlinear robust adaptive tracking control of a quadrotor UAV via immersion and invariance methodology," *IEEE Trans. Ind. Electron.*, vol. 62, no. 5, pp. 2891–2902, May 2015.

[8] Y.-C. Choi and H.-S. Ahn, "Nonlinear control of quadrotor for point tracking: Actual implementation and experimental tests," *IEEE/ASME Trans. Mechatronics*, vol. 20, no. 3, pp. 1179–1192, Jun. 2015.

[9] D. Lee, H. Jin Kim, and S. Sastry, "Feedback linearization vs. adaptive sliding mode control for a quadrotor helicopter," *Int. J. Control, Autom. Syst.*, vol. 7, no. 3, pp. 419–428, Jun. 2009.

[10] A. Benallegue, A. Mokhtari, and L. Fridman, "Feedback linearization and high order sliding mode observer for a quadrotor UAV," in *Proc. Int. Workshop Variable Struct. Syst. (VSS)*, 2006, pp. 365–372.

[11] Z. Hou, I. Fantoni, and A. ZAVALA-RIO, "Modeling and decentralized control for the multiple UAVs formation based on Lyapunov design and redesign," *IFAC Proc. Volumes*, vol. 46, no. 30, pp. 337–344, 2013.

[12] G. V. Raffo and M. M. de Almeida, "Nonlinear robust control of a quadrotor UAV for load transportation with swing improvement," in *Proc. Amer. Control Conf. (ACC)*, Jul. 2016, pp. 3156–3162.

[13] H. Liu, J. Xi, and Y. Zhong, "Robust attitude stabilization for nonlinear quadrotor systems with uncertainties and delays," *IEEE Trans. Ind. Electron.*, vol. 64, no. 7, pp. 5585–5594, Jul. 2017.

[14] R. Xu and U. Ozguner, "Sliding mode control of a quadrotor helicopter," in *Proc. 45th IEEE Conf. Decis. Control*, Dec. 2006, pp. 4957–4962.

[15] F. Chen, R. Jiang, K. Zhang, B. Jiang, and G. Tao, "Robust backstepping sliding-mode control and observer-based fault estimation for a quadrotor UAV," *IEEE Trans. Ind. Electron.*, vol. 63, no. 8, pp. 5044–5056, Aug. 2016.

[16] E.-H. Zheng, J.-J. Xiong, and J.-L. Luo, "Second order sliding mode control for a quadrotor UAV," *ISA Trans.*, vol. 53, no. 4, pp. 1350–1356, Jul. 2014.

[17] H. Le Nhu Ngoc Thanh and S. K. Hong, "Quadcopter robust adaptive second order sliding mode control based on PID sliding surface," *IEEE Access*, vol. 6, pp. 66850–66860, 2018.

[18] J.-J. Xiong and G.-B. Zhang, "Global fast dynamic terminal sliding mode control for a quadrotor UAV," *ISA Trans.*, vol. 66, pp. 233–240, Jan. 2017.

[19] G. V. Raffo, M. G. Ortega, and F. R. Rubio, "Backstepping/nonlinear H_∞ control for path tracking of a quadrotor unmanned aerial vehicle," in *Proc. Amer. Control Conf.*, Jun. 2008, pp. 3356–3361.

[20] C. Ha, Z. Zuo, F. B. Choi, and D. Lee, "Passivity-based adaptive backstepping control of quadrotor-type UAVs," *Robot. Auto. Syst.*, vol. 62, no. 9, pp. 1305–1315, Sep. 2014.

[21] J. Hu and H. Zhang, "Immersion and invariance based command-filtered adaptive backstepping control of VTOL vehicles," *Automatica*, vol. 49, no. 7, pp. 2160–2167, Jul. 2013.

[22] D. Kapoor, D. Deb, A. Sahai, and H. Bangar, "Adaptive failure compensation for coaxial rotor helicopter under propeller failure," in *Proc. Amer. Control Conf. (ACC)*, Jun. 2012, pp. 2539–2544.

[23] D. Deb, G. Tao, J. O. Burkholder, and D. R. Smith, "Adaptive compensation control of synthetic jet actuator arrays for airfoil virtual shaping," *J. Aircr.*, vol. 44, no. 2, pp. 616–626, Mar. 2007.

[24] D. Deb, G. Tao, and J. O. Burkholder, "Adaptive approximation based compensation of synthetic jet actuator nonlinearities for aircraft control," in *Proc. AIAA Guid., Navigat., Control Conf.*, 2007.

[25] T. Lee, "Robust adaptive attitude tracking on SO(3) with an application to a quadrotor UAV," *IEEE Trans. Control Syst. Technol.*, vol. 21, no. 5, pp. 1924–1930, Sep. 2013.

[26] S. H. Jeong and S. Jung, "Experimental studies of a disturbance observer for attitude control of a quad-rotor system," in *Proc. IEEE Int. Conf. Automat. Syst.*, Oct. 2012, pp. 579–583.

[27] F. Chen, W. Lei, K. Zhang, G. Tao, and B. Jiang, "A novel nonlinear resilient control for a quadrotor UAV via backstepping control and nonlinear disturbance observer," *Nonlinear Dyn.*, vol. 85, no. 2, pp. 1281–1295, Apr. 2016.

[28] L. Besnard, Y. B. Shtessel, and B. Landrum, "Quadrotor vehicle control via sliding mode controller driven by sliding mode disturbance observer," *J. Franklin Inst.*, vol. 349, no. 2, pp. 658–684, Mar. 2012.

[29] Y. Chang, Y. Wang, F. E. Alsaadi, and G. Zong, "Adaptive fuzzy output-feedback tracking control for switched stochastic pure-feedback nonlinear systems," *Int. J. Adapt. Control*, vol. 33, no. 10, pp. 1567–1582, Oct. 2019.

[30] Z.-M. Li, X.-H. Chang, and J. H. Park, "Quantized static output feedback fuzzy tracking control for discrete-time nonlinear networked systems with asynchronous event-triggered constraints," *IEEE Trans. Syst., Man, Cybern. Syst.*, early access, Aug. 15, 2019, doi: 10.1109/TSMC.2019.2931530.

[31] L. Ma, X. Huo, X. Zhao, and G. Zong, "Adaptive fuzzy tracking control for a class of uncertain switched nonlinear systems with multiple constraints: A small-gain approach," *Int. J. Fuzzy Syst.*, vol. 21, no. 8, pp. 2609–2624, Oct. 2019.

[32] H. Yang, L. Cheng, Y. Xia, and Y. Yuan, "Active disturbance rejection attitude control for a dual closed-loop quadrotor under gust wind," *IEEE Trans. Control Syst. Technol.*, vol. 26, no. 4, pp. 1400–1405, Jul. 2018.

[33] D. Shi, Z. Wu, and W. Chou, "Generalized extended state observer based high precision attitude control of quadrotor vehicles subject to wind disturbance," *IEEE Access*, vol. 6, pp. 32349–32359, 2018.

[34] R. Zhang, Q. Quan, and K.-Y. Cai, "Attitude control of a quadrotor aircraft subject to a class of time-varying disturbances," *IET Control Theory Appl.*, vol. 5, no. 9, pp. 1140–1146, Jun. 2011.

[35] M. He and J. He, "Extended state observer-based robust backstepping sliding mode control for a small-size helicopter," *IEEE Access*, vol. 6, pp. 33480–33488, 2018.

[36] J. Sun, Y. Wang, Y. Yu, and C. Sun, "Nonlinear robust compensation method for trajectory tracking control of quadrotors," *IEEE Access*, vol. 7, pp. 26766–26776, 2019.

[37] T. Jiang, D. Lin, and T. Song, "Finite-time backstepping control for quadrotors with disturbances and input constraints," *IEEE Access*, vol. 6, pp. 62037–62049, 2018.

[38] X. Wang and B. Shirinzadeh, "Nonlinear augmented observer design and application to quadrotor aircraft," *Nonlinear Dyn.*, vol. 80, no. 3, pp. 1463–1481, Feb. 2015.

[39] F. Blanchini, T. Parisini, F. A. Pellegrino, and G. Pin, "High-gain adaptive control: A derivative-based approach," *IEEE Trans. Autom. Control*, vol. 54, no. 9, pp. 2164–2169, Sep. 2009.

[40] H. K. Khalil, "High-gain observers in feedback control: Application to permanent magnet synchronous motors," *IEEE Control Syst. Mag.*, vol. 37, no. 3, pp. 25–41, Jun. 2017.

[41] Y. Gui, W. Kim, and C. C. Chung, "Passivity-based control with nonlinear damping for type 2 STATCOM systems," *IEEE Trans. Power Syst.*, vol. 31, no. 4, pp. 2824–2833, Jul. 2016.

[42] R. Kosut, "Design of linear systems with saturating linear control and bounded states," *IEEE Trans. Autom. Control*, vol. 28, no. 1, pp. 121–124, Jan. 1983.

[43] H. Khalil, *Nonlinear Systems*, 3rd ed. Upper Saddle River, NJ, USA: Prentice-Hall, 2002.

[44] M. Krstic, I. Kanellakopoulos, and P. Kokotovic, *Nonlinear and Adaptive Control Design*. New York, NY, USA: Wiley, 1995.

SESUN YOU received the B.S. degree from the School of Energy Systems Engineering, Chung-Ang University, Seoul, South Korea, in 2020. He is currently pursuing the Ph.D. degree with the Department of Energy System Engineering, Chung-Ang University. His research interests include nonlinear control, adaptive control, neural control, intelligent control for nonlinear systems, and their industrial applications.

KWANYEON KIM is currently pursuing the degree with the School of Energy System Engineering, Chung-Ang University, Seoul, South Korea. His research interests include quadrotor control, neural control, intelligent control for nonlinear systems, and their industrial applications.

JUN MOON (Senior Member, IEEE) received the B.S. degree in electrical and computer engineering and the M.S. degree in electrical engineering from Hanyang University, Seoul, South Korea, in 2006 and 2008, respectively, and the Ph.D. degree in electrical and computer engineering from the University of Illinois at Urbana–Champaign, USA, in 2015. He is currently an Associate Professor with the Department of Electrical Engineering, Hanyang University. From February 2008 to June 2011, he was a Researcher at the Agency for Defense Development (ADD), South Korea. From February 2016 to 2019, he was an Assistant Professor with the School of Electrical and Computer Engineering, Ulsan National Institute of Science and Technology (UNIST), South Korea. From March 2019 to August 2020, he was an Assistant Professor and an Associate Professor with the School of Electrical and Computer Engineering, University of Seoul, South Korea. His research interests include stochastic games, control and estimation, mean field games, distributed optimal control, networked control systems, and control of unmanned vehicles. He was a recipient of the Fulbright Graduate Study Award in 2011.

WONHEE KIM (Member, IEEE) received the B.S. and M.S. degrees in electrical and computer engineering and the Ph.D. degree in electrical engineering from Hanyang University, Seoul, South Korea, in 2003, 2005, and 2012, respectively. From 2005 to 2007, he was with Samsung Electronics Company, Suwon, South Korea. In 2012, he was with the Power and Industrial Systems Research and Development Center, Hyosung Corporation, Seoul. In 2013, he was a Postdoctoral Researcher with the Institute of Nano Science and Technology, Hanyang University, and a Visiting Scholar with the Department of Mechanical Engineering, University of California at Berkeley, Berkeley, CA, USA. From 2014 to 2016, he was with the Department of Electrical Engineering, Dong-A University, Busan, South Korea. He is currently an Associate Professor with the School of Energy Systems Engineering, Chung-Ang University, Seoul. His current research interests include nonlinear control and nonlinear observers, as well as their industrial applications. He has served as an Associate Editor for IEEE Access and the *Journal of Electrical Engineering and Technology*.